






Polaronic enhancement of second-harmonic generation in lithium niobate

Agnieszka L. Kozub ^{*}, Arno Schindlmayr , Uwe Gerstmann , and Wolf Gero Schmidt 
 Universität Paderborn, Department Physik, 33095 Paderborn, Germany

 (Received 11 June 2021; revised 5 October 2021; accepted 3 November 2021; published 18 November 2021)

Density-functional theory within a Berry-phase formulation of the dynamical polarization is used to determine the second-order susceptibility $\chi^{(2)}$ of lithium niobate (LiNbO₃). Defect-trapped polarons and bipolarons are found to strongly enhance the nonlinear susceptibility of the material, in particular when localized at Nb_V-V_{Li} defect pairs. This is essentially a consequence of the formation of polaronic states inside the band gap. The population of these levels, for example, by illumination leads to strongly enhanced $\chi^{(2)}$ coefficients and thus allows for the spatial and transient modification of the second-harmonic generation in macroscopic samples.

DOI: [10.1103/PhysRevB.104.174110](https://doi.org/10.1103/PhysRevB.104.174110)

I. INTRODUCTION

The arbitrary control of electromagnetic waves is a key aim of photonic research. This requires the engineering of optical coefficients, e.g., by doping, strain, or electric fields [1–5]. Photorefractive materials like lithium niobate (LiNbO₃, LN) that respond to light by altering their refractive index are of particular interest in this context [6,7]. Lithium niobate is used, e.g., for optical waveguides, optical modulators, photonic integrated circuits, and nonvolatile holographic storage [8,9].

The optical properties of LN are profoundly affected by polarons, i.e., electrons excited to a state close to the edge of the conduction band that get dressed with a cloud of virtual polar phonons [10–14] (see Fig. 1). Free small polarons (F) are the simplest polaron species in LN. They are formed by extra electrons trapped at regular Nb_{Nb} ions of the LN lattice. Bound polarons (P) and bound bipolarons (B) are formed by single electrons and pairs of electrons, respectively, localized at point defects. These defects are related to excess Nb compensating the lithium deficit observed in the congruently melting composition of lithium niobate. Single polarons (F and P) are usually found as metastable states upon optical excitation and may combine into bipolarons. The latter also result from thermal or electrochemical reduction and can be thermally or optically split into single-electron polarons [10,12,15]. Optical absorption peaks at about 0.9, 1.6, and 2.5 eV are assigned to F [16], P [17], and B [18], respectively. The direct band gap of LN derived from optical experiments is 3.78 eV [19].

Second-harmonic generation (SHG) is an optical process in which light doubles its frequency by interaction with a nonlinear material. Specifically, the second-order polarization induced by a monochromatic electric field $\mathbf{E}(t) = E_0 \exp(-i\omega t)$ is given as

$$P_i^{(2)}(2\omega) = \epsilon_0 \sum_{j,k} \chi_{ijk}^{(2)}(2\omega, \omega, \omega) E_j(\omega) E_k(\omega), \quad (1)$$

where $\chi_{ijk}^{(2)}$ is a third-rank tensor describing the material's second-order susceptibility [20,21], with i, j , and k referring to the Cartesian coordinates. Thus, tailoring of $\chi^{(2)}$ allows for controlling the SHG [22,23]. Although polarons have been known for a long time to cause various optical nonlinearities [24], such as green-induced infrared absorption in LN [25] and the enhancement of the third-order susceptibility $\chi^{(3)}$ in organic materials [26], their influence on $\chi^{(2)}$ in LN is essentially unknown. In the present work, we show by means of first-principles calculations that electron polarons cause a strong enhancement of $\chi^{(2)}$ for photon energies in the lower half of the LN band gap. Given that the polaron density may be modified by dopants that can be positioned during fabrication [10,27] as well as by optical excitation [28,29], polarons provide a way to control spatially and transiently the second-harmonic generation in LN.

II. COMPUTATIONAL METHODS

In detail, we use density-functional theory (DFT) to perform electronic-structure calculations based on the QUANTUM ESPRESSO [30,31] implementation. The generalized gradient approximation is employed using the PBEsol functional [32], a PBE functional optimized for solids. In order to account for the strong localization of the Nb $4d$ electrons, we employ the DFT+ U scheme [33]. Following Ref. [34], self-consistently determined U values are used, i.e., 4.7 eV for the regular Nb atoms (also those with free polarons) and 5.2 eV for Nb_{Li} antisite and Nb_V interstitial atoms. Spin-polarized calculations are performed for single P and F polarons, which are formed by unpaired electrons, whereas bipolarons B are characterized by diamagnetic spin-singlet states. The nonlinear susceptibilities are obtained from the real-time evolution of the Bloch electrons in a uniform time-dependent electric field following the Berry-phase approach proposed by Attaccalite and Grüning [35]. In this method, the time-dependent polarization is computed from the evolution of valence states $|v_{\mathbf{k}}\rangle$, described by the equations of motion

$$i\hbar \frac{\partial}{\partial t} |v_{\mathbf{k}}\rangle = (H_{\mathbf{k}}^{\text{sys}} + i\mathbf{E} \cdot \tilde{\delta}_{\mathbf{k}}) |v_{\mathbf{k}}\rangle, \quad (2)$$

^{*}agnieszka.kozub@uni-paderborn.de

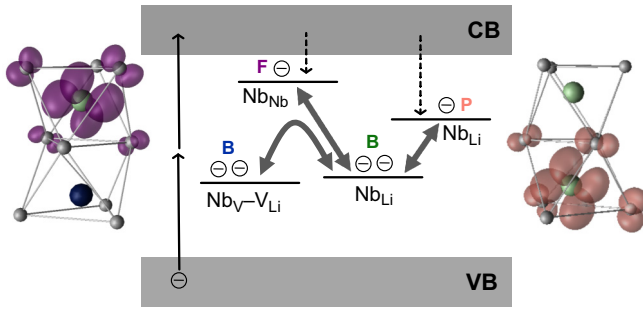


FIG. 1. Schematic illustration of electron polaron states in lithium niobate. Band-to-band excitation and subsequent carrier localization lead to the formation of free (F) and bound (P) polarons, which combine to bipolarons (B). Bipolarons may transform structurally or dissociate into single-electron polarons. The charge densities of free and bound polaron orbitals in the tilted ground-state configurations are shown on the left and right, respectively. CB labels conduction band and VB labels valence band. See Fig. 2 for complete structures and the notation of atoms.

where $H_{\mathbf{k}}^{\text{sys}}$ stands for the system Hamiltonian. In the majority of this work, we used the independent-particle approximation, where $H_{\mathbf{k}}^{\text{sys}}$ is taken to be the unperturbed Kohn-Sham Hamiltonian $H_{\mathbf{k}}^{\text{KS}}$. The quasiparticle correction to the band structure may be included by adding the scissors operator $\Delta H_{\mathbf{k}}$ to $H_{\mathbf{k}}^{\text{KS}}$. The term $\mathbf{E} \cdot \tilde{\delta}_{\mathbf{k}}$ in Eq. (2) corresponds to the coupling with the external electric field \mathbf{E} . Finally, $\chi^{(2)}$ is derived from the power series expansion of the calculated polarization $\mathbf{P} = \chi^{(1)}\mathbf{E} + \chi^{(2)}\mathbf{E}\mathbf{E} + \dots$.

Stoichiometric LN crystallizes in a rhombohedral unit cell. The oxygen atoms form octahedra that are alternately occupied by Li or Nb or are empty [see Fig. 2(a)]. The present polaron calculations are based on previously established structure models [34], which account for both the measured optical absorption peaks and the electron-paramagnetic-resonance data. As illustrated in Fig. 2, we consider free polarons, in

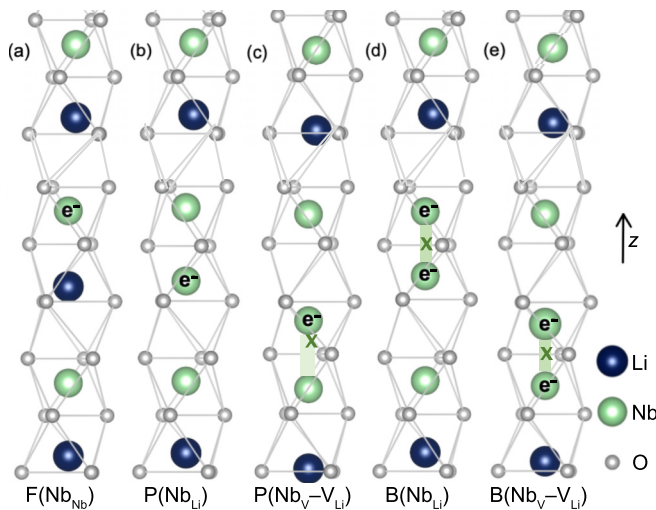


FIG. 2. (a) Free polarons, (b) and (c) bound polarons, and (d) and (e) bipolarons in LiNbO_3 defect structures. Trapped electrons (e^-) as well as their orbital hybridization along the z axis and the center of the polaronic charges (x) are indicated (see Fig. 3).

which the excess electron is bound to a regular Nb_{Nb} ion [Fig. 2(a)]; bound polarons with the excess electron at the Nb_{Li} antisite defect [Fig. 2(b)]; bound polarons with the excess electron at the Nb_{V} interstitial of the $\text{Nb}_{\text{V}}\text{-V}_{\text{Li}}$ defect pair [Fig. 2(c)]; and bipolarons, in which one of the excess electrons is at the defect niobium atom of the Nb_{Li} antisite defect [Fig. 2(d)] or the $\text{Nb}_{\text{V}}\text{-V}_{\text{Li}}$ defect pair [Fig. 2(e)] and the second is at the neighboring Nb atom. The structures shown in Figs. 2(a)–2(c) are studied in both the axially symmetric and quasi-Jahn-Teller distorted (tilted) configurations [34]. The structures in Figs. 2(d) and 2(e) have axial symmetry. In this case, the niobium atoms carrying the excess electrons shift only along the crystal z axis, preserving the threefold rotational symmetry, while in the tilted configurations, the polaron-carrying atoms are additionally displaced in the xy plane, which results in cloverleaf-shaped orbitals for the excess electrons [36]. The defect structures are embedded in 80-atom supercells as described in Ref. [36], and a $3 \times 3 \times 3$ Γ -centered \mathbf{k} -point sampling is used for the real-time propagation. For defect-free stoichiometric LN, we choose the 10-atom unit cell and a $6 \times 6 \times 6$ Γ -centered \mathbf{k} -point grid instead. In all calculations, we use a plane wave cutoff of 85 Ry. To calculate second-order susceptibility $\chi^{(2)}$, we numerically integrate Eq. (2) for a time interval of 53 fs with a time step of $\Delta t = 0.01$ fs and damping equal to 0.2 eV. The dephasing time, after which $\chi^{(2)}$ is obtained, is set to 40 fs.

III. RESULTS AND DISCUSSION

Figure 3 shows the modulus of the calculated second-order susceptibility as a function of the incident photon energy. Unless stated otherwise, we plot the most frequently measured tensor element $|\chi_{zzz}^{(2)}(\omega)|$. The calculations for the stoichiometric bulk material agree well with previous calculations [37] and reproduce the order of magnitude of the experimental data [38]. The small $|\chi_{zzz}^{(2)}(\omega)|$ values for energies in the lower half of the LN band gap are strongly enhanced upon bipolaron formation and for $\text{P}(\text{Nb}_{\text{V}}\text{-V}_{\text{Li}})$ with axial symmetry. In fact, the values obtained here for the supercells containing polarons or bipolarons, $|\chi_{zzz}^{(2)}| \approx 200 \text{ pmV}^{-1}$, are comparable to the value of GaAs in the energy region above the band gap, which is known as one of the largest values reported for solid-state systems [20]. In the case of $\text{B}(\text{Nb}_{\text{V}}\text{-V}_{\text{Li}})$, where the enhancement is most pronounced, we also show the other tensor elements of the second-order susceptibility that are nonzero in the trigonal symmetry [39] characteristic of stoichiometric LN and of polaron states with axial symmetry: $|\chi_{yxx}^{(2)}(\omega)|$, $|\chi_{yyz}^{(2)}(\omega)|$, and $|\chi_{zxx}^{(2)}(\omega)|$. These are much smaller than $|\chi_{zzz}^{(2)}(\omega)|$ in the low-energy region, which also holds for the other polaron species.

According to Miller's rule [20,40], the quantity

$$\Delta(\omega) = \chi^{(2)}(2\omega) / \{\chi^{(1)}(2\omega)[\chi^{(1)}(\omega)]^2\} \quad (3)$$

should be a slowly varying function of ω . It applies to frequency doubling and allows, in many cases, to relate linear and nonlinear susceptibilities of noncentrosymmetric crystals. As can be seen in Fig. 4, Miller's rule holds for stoichiometric LN but is clearly violated for bipolarons and bound polarons localized at $\text{Nb}_{\text{V}}\text{-V}_{\text{Li}}$. These systems are characterized by a strong bond-charge acentricity and are not well

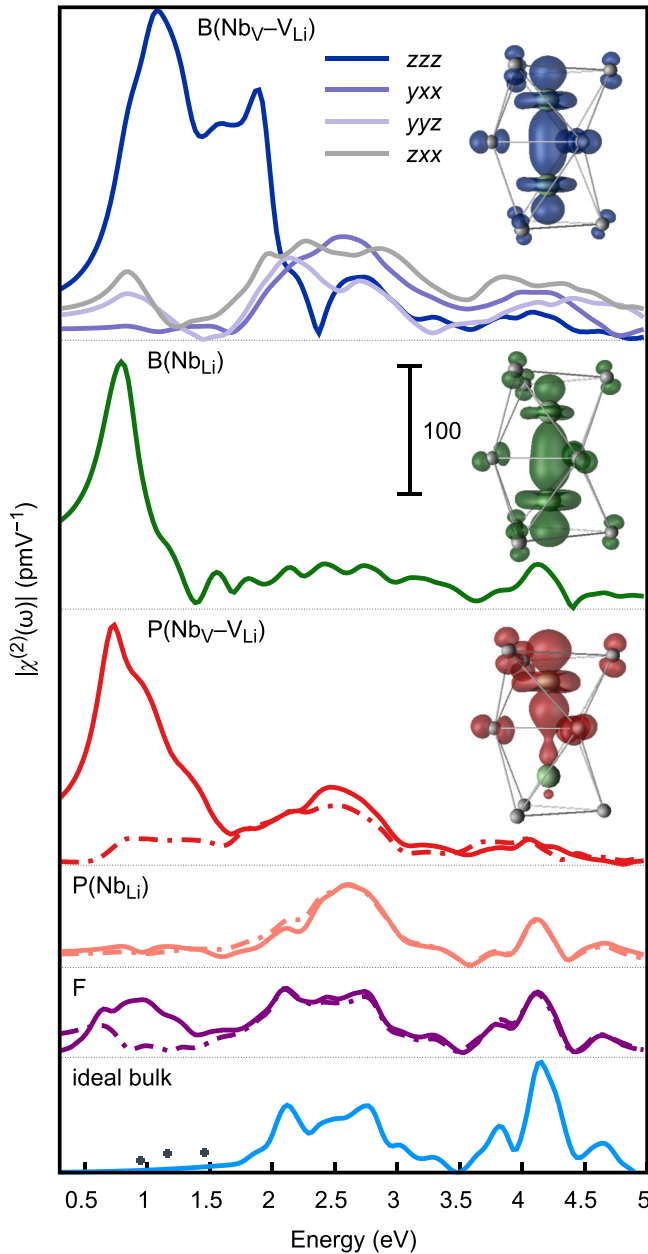


FIG. 3. Values of $|\chi^{(2)}(\omega)|$ calculated for ideal stoichiometric LN as well as for supercells that contain electron polarons. Solid lines correspond to structures with axial symmetry; dashed-dotted lines correspond to tilted configurations. For $B(Nb_V-V_{Li})$ all nonvanishing $\chi^{(2)}(\omega)$ components are exemplarily given; for the others only the dominant zzz contribution is shown. The black symbols in the bottom panel represent experimental data for congruent $LiNbO_3$ [38].

described within the classical anharmonic oscillator model [20,41]. Indeed, a common feature of all the systems with strongly enhanced $|\chi_{zzz}^{(2)}(\omega)|$ is a pronounced hybridization of the polaron orbital at the defect niobium atom with the neighboring atom along the z direction [36], as displayed in the inset of Fig. 3. This hybridization shifts the center of the polaronic charge away from its position in ideal stoichiometric LN, as indicated in Fig. 2.

What precisely is the microscopic origin of the large optical nonlinearities associated with some polaron species? In

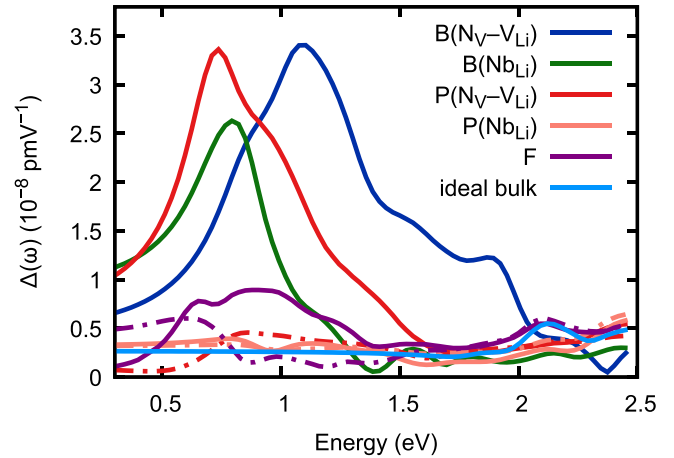


FIG. 4. Check of Miller's rule for bulk $LiNbO_3$ and for crystal structures containing electron polarons. Solid lines correspond to the structures with axial symmetry; dashed-dotted lines correspond to the tilted configuration.

order to answer this question, we separate the influence of the defect formation and the polaronic excitation, i.e., the trapping of additional electrons and the associated lattice relaxation, for the bipolarons as well as $P(Nb_V-V_{Li})$. Figure 5 (solid black lines) shows that the point defects themselves modify $|\chi_{zzz}^{(2)}|$ only slightly, at least for low photon energies. However, upon polaronic excitation, the low-energy susceptibility is much enhanced, in analogy to the polaron-related additional absorption peaks in the linear optical response [16–18]. This enhancement either could be due to new electronic transitions related to the polaron states or might be caused by the additional lattice deformation accompanying the polaron formation, simply relaxing the optical selection rules. To discriminate between these two possibilities, we perform calculations for supercells that exhibit the (bi)polaron geometries but contain no excess electrons. The corresponding spectra are plotted with colored dashed lines in Fig. 5. It can be seen that in the case of bipolarons, both the electronic occupation and the lattice relaxation contribute to $\chi^{(2)}$ enhancement, whereas the electronic effects dominate for bound polarons. For $B(Nb_V-V_{Li})$, the SHG enhancement is not limited to the energy region around 1 eV but extends up to 2 eV, where an additional second peak can be identified. This peak originates from transitions into empty Nb $4d$ states close to the conduction-band edge and shows up at twice the energy already in the $B(Nb_V-V_{Li})$ linear optical response [36]. Indeed, as shown by the dash-dotted black line in Fig. 5, it is predicted by Miller's rule applied to $\chi^{(1)}$. For $P(Nb_{Li})$ and F the lattice distortion related to the polaron formation is much smaller. Therefore, these structures do not show a significant $\chi^{(2)}$ enhancement.

How important is the polaronic SHG enhancement for real samples? Merschjann and coworkers [42] determined polaron densities in congruently melting $LiNbO_3$ by time-resolved pump-multiprobe spectroscopy. They obtained a steady-state number density of bipolarons of $6.7 \times 10^{23} \text{ m}^{-3}$ at room temperature without illumination, which can be drastically enhanced by optical excitation. Electron polarons in lithium niobate are generated optically within a few hundred fem-

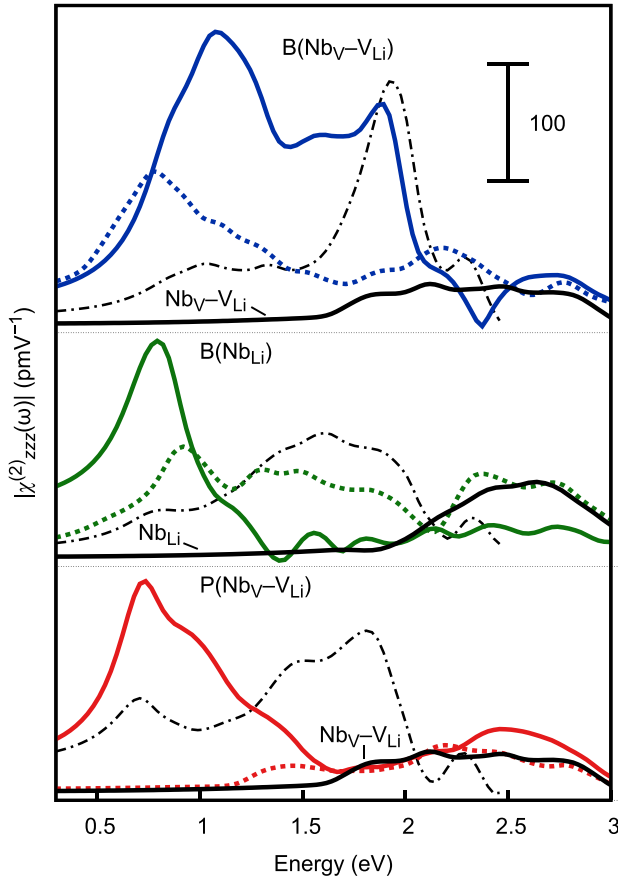


FIG. 5. $|\chi_{zzz}^{(2)}(\omega)|$ calculated for supercells containing bare defects (solid black lines), defect-localized (bi)polarons (solid colored lines), and polaron structures without trapped electrons (dashed colored lines). The dash-dotted black line represents $|\chi_{zzz}^{(2)}(\omega)|$ estimated from Miller's rule (in arbitrary units).

toseconds [28,29]. In this way, concentrations far higher than in the steady state can be achieved. Buse and coworkers [28], for example, determined a polaron density of $4.4 \times 10^{24} \text{ m}^{-3}$. This value is used for an order-of-magnitude estimate for the bipolaron-induced $|\chi_{zzz}^{(2)}(\omega)|$ change in Fig. 6. Obviously, $|\chi_{zzz}^{(2)}|$ changes of the order of several percent can be expected to result from optical excitation of LN samples even without a particular material modification that gives rise to additional antisites.

In order to probe the influence of defect complex formation on the polaron-induced SHG signal, we study structures in which up to three $B(\text{Nb}_V\text{-V}_{\text{Li}})$ or $B(\text{Nb}_{\text{Li}})$ polarons are contained in the 80-atom cell. No significant modification of the defect-density normalized $\chi^{(2)}$ values is found, indicating that, in particular, no signal cancellation is to be expected.

A word of caution is in order considering the present DFT calculations. Optical excitations are known to be influenced by electronic many-body effects beyond DFT [43–49]. In order to probe their influence, we add a scissors-operator correction to the effective Hamiltonian for the Bloch electrons (see the dashed line in Fig. 6). Its size is determined by *GW* calculations [34] that predict a blueshift of 0.6 eV

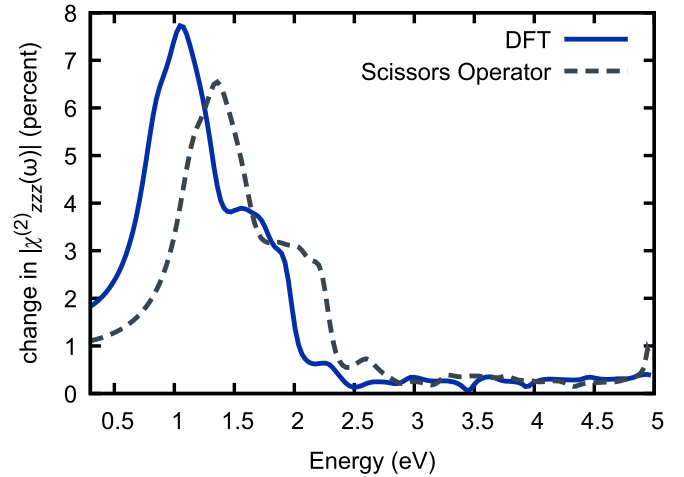


FIG. 6. Relative change in $|\chi_{zzz}^{(2)}(\omega)|$ due to $B(\text{Nb}_V\text{-V}_{\text{Li}})$ formation in bulk LiNbO_3 , assuming a density of $4.4 \times 10^{24} \text{ m}^{-3}$. In addition to calculations within the independent-particle approximation (DFT), the estimate for the influence of self-energy corrections (scissors operator) is shown (see text).

for transitions from the $B(\text{Nb}_V\text{-V}_{\text{Li}})$ defect state to the LN conduction-band minimum compared to DFT. As a consequence, we observe a blueshift and a slight weakening of the SHG signal. As excitonic effects are expected to redshift and increase the SHG spectral features [43–46], the dashed line in Fig. 6 represents an upper limit for the excitation energies and a lower limit for the SHG enhancement that can be expected to result from the bipolaron formation. Therefore, the polaronic effect on $\chi^{(2)}$ predicted here from DFT is robust with respect to many-body effects.

IV. CONCLUSIONS

In summary, the present density-functional calculations predict a strong $\chi^{(2)}$ enhancement in lithium niobate upon formation of bound (bi)polarons. It is caused primarily by the occupation of the relaxation-induced polaronic defect levels inside the band gap. Further details of the SHG enhancement depend sensitively on the relative position of the polaronic charge density with respect to the neighboring cations of the ferroelectric host material. The polaron density in real samples depends on the availability of possible lattice trapping sites, which may be locally modified by doping [10]. In addition, it can be strongly increased by optical excitation of the sample. The polaronic enhancement of the nonlinear optical coefficients predicted here thus suggests a way to control second-harmonic generation beyond strain or external electric fields.

ACKNOWLEDGMENTS

The DFG (TRR 142, Project No. 231447078) is acknowledged for financial support. We thank the Paderborn Center for Parallel Computing (PC²) and the Höchstleistungs-Rechenzentrum Stuttgart (HLRS) for grants of high-performance computer time.

- [1] M. Cazzanelli, F. Bianco, E. Borga, G. Pucker, M. Ghulinyan, E. Degoli, E. Luppi, V. Véniard, S. Ossicini, D. Modotto, S. Wabnitz, R. Pierobon, and L. Pavesi, *Nat. Mater.* **11**, 148 (2012).
- [2] R. S. Jacobsen, K. N. Andersen, P. I. Borel, J. Fage-Pedersen, L. H. Frandsen, O. Hansen, M. Kristensen, A. V. Lavrinenko, G. Moulin, H. Ou, C. Peucheret, B. Zsigri, and A. Bjarklev, *Nature (London)* **441**, 199 (2006).
- [3] T. Zhang, B. Wang, Y.-Q. Zhao, S.-Q. Fang, D.-C. Ma, and Y.-H. Xu, *Mater. Chem. Phys.* **88**, 97 (2004).
- [4] K. L. Seyler, J. R. Schaibley, P. Gong, P. Rivera, A. M. Jones, S. Wu, J. Yan, D. G. Mandrus, W. Yao, and X. Xu, *Nat. Nanotechnol.* **10**, 407 (2015).
- [5] J.-M. Yi, D. Wang, F. Schwarz, J. Zhong, A. Chimeh, A. Korte, J. Zhan, P. Schaaf, E. Runge, and C. Lienau, *ACS Photonics* **6**, 2779 (2019).
- [6] J. Frejlich, *Photorefractive Materials: Fundamental Concepts, Holographic Recording and Materials Characterization* (Wiley, Hoboken, NJ, 2006).
- [7] *Photorefractive Materials and Their Applications I: Fundamental Phenomena*, edited by P. Günter and J. P. Huignard (Springer, New York, 2014).
- [8] L. Hesselink, S. S. Orlov, A. Liu, A. Akella, D. Lande, and R. R. Neurgaonkar, *Science* **282**, 1089 (1998).
- [9] K. Buse, A. Adibi, and D. Psaltis, *Nature (London)* **393**, 665 (1998).
- [10] O. F. Schirmer, M. Imlau, C. Merschjann, and B. Schoke, *J. Phys.: Condens. Matter* **21**, 123201 (2009).
- [11] F. Luedtke, K. Buse, and B. Sturman, *Phys. Rev. Lett.* **109**, 026603 (2012).
- [12] M. Imlau, H. Badorreck, and C. Merschjann, *Appl. Phys. Rev.* **2**, 040606 (2015).
- [13] A. Krampf, S. Messerschmidt, and M. Imlau, *Sci. Rep.* **10**, 11397 (2020).
- [14] Y. Furukawa, M. Sato, K. Kitamura, Y. Yajima, and M. Minakata, *J. Appl. Phys.* **72**, 3250 (1992).
- [15] C. Merschjann, D. Berben, M. Imlau, and M. Wöhlecke, *Phys. Rev. Lett.* **96**, 186404 (2006).
- [16] B. Faust, H. Müller, and O. F. Schirmer, *Ferroelectrics* **153**, 297 (1994).
- [17] K. L. Sweeney and L. E. Halliburton, *Appl. Phys. Lett.* **43**, 336 (1983).
- [18] J. Koppitz, O. F. Schirmer, and A. I. Kuznetsov, *Europhys. Lett.* **4**, 1055 (1987).
- [19] A. Dhar and A. Mansingh, *J. Appl. Phys.* **68**, 5804 (1990).
- [20] R. W. Boyd, *Nonlinear Optics* (Academic, London, 2020).
- [21] J. E. Sipe and A. I. Shkrebtii, *Phys. Rev. B* **61**, 5337 (2000).
- [22] U. R. Meza, B. S. Mendoza, and W. L. Mochán, *Phys. Rev. B* **99**, 125408 (2019).
- [23] C. B. Uzundal *et al.*, *Phys. Rev. Lett.* (to be published), [arXiv:2104.01313](https://arxiv.org/abs/2104.01313).
- [24] K.-X. Guo and C.-Y. Chen, *Solid State Commun.* **99**, 363 (1996).
- [25] Y. Furukawa, K. Kitamura, A. Alexandrovski, R. K. Route, M. M. Fejer, and G. Foulon, *Appl. Phys. Lett.* **78**, 1970 (2001).
- [26] C. Taliani, G. Ruani, R. Zamboni, F. Kajzar, L. Yang, R. Dorsinville, R. R. Alfano, and R. Tubino, in *Organic Molecules for Nonlinear Optics and Photonics*, edited by J. Messier, F. Kajzar, and P. Prasad (Springer, Dordrecht, 1991), pp. 301–312.
- [27] J. J. Amodei and D. L. Staebler, *Appl. Phys. Lett.* **18**, 540 (1971).
- [28] O. Beyer, D. Maxein, T. Woike, and K. Buse, *Appl. Phys. B* **83**, 527 (2006).
- [29] H. Badorreck, S. Nolte, F. Freytag, P. Bäune, V. Dieckmann, and M. Imlau, *Opt. Mater. Express* **5**, 2729 (2015).
- [30] P. Giannozzi *et al.*, *J. Phys.: Condens. Matter* **21**, 395502 (2009).
- [31] P. Giannozzi *et al.*, *J. Phys.: Condens. Matter* **29**, 465901 (2017).
- [32] M. Friedrich, A. Riefer, S. Sanna, W. G. Schmidt, and A. Schindlmayr, *J. Phys.: Condens. Matter* **27**, 385402 (2015).
- [33] M. Cococcioni and S. de Gironcoli, *Phys. Rev. B* **71**, 035105 (2005).
- [34] F. Schmidt, A. L. Kozub, T. Biktagirov, C. Eigner, C. Silberhorn, A. Schindlmayr, W. G. Schmidt, and U. Gerstmann, *Phys. Rev. Research* **2**, 043002 (2020).
- [35] C. Attacalite and M. Grüning, *Phys. Rev. B* **88**, 235113 (2013).
- [36] F. Schmidt, A. L. Kozub, U. Gerstmann, W. G. Schmidt, and A. Schindlmayr, *Crystals* **11**, 542 (2021).
- [37] A. Riefer, S. Sanna, A. Schindlmayr, and W. G. Schmidt, *Phys. Rev. B* **87**, 195208 (2013).
- [38] I. Shoji, T. Kondo, A. Kitamoto, M. Shirane, and R. Ito, *J. Opt. Soc. Am. B* **14**, 2268 (1997).
- [39] M. Trzeciński, A. Dähn, and W. Hübner, *Phys. Rev. B* **60**, 1144 (1999).
- [40] R. C. Miller, *Appl. Phys. Lett.* **5**, 17 (1964).
- [41] B. F. Levine, *Phys. Rev. B* **7**, 2600 (1973).
- [42] C. Merschjann, B. Schoke, D. Conradi, M. Imlau, G. Corradi, and K. Polgár, *J. Phys.: Condens. Matter* **21**, 015906 (2008).
- [43] E. K. Chang, E. L. Shirley, and Z. H. Levine, *Phys. Rev. B* **65**, 035205 (2001).
- [44] R. Leitsmann, W. G. Schmidt, P. H. Hahn, and F. Bechstedt, *Phys. Rev. B* **71**, 195209 (2005).
- [45] M. L. Trolle, G. Seifert, and T. G. Pedersen, *Phys. Rev. B* **89**, 235410 (2014).
- [46] A. Riefer and W. G. Schmidt, *Phys. Rev. B* **96**, 235206 (2017).
- [47] P. Deák, *Physica B (Amsterdam, Neth.)* **535**, 35 (2018).
- [48] E. Cadelano, J. Furthmüller, G. Cappellini, and F. Bechstedt, *J. Phys.: Condens. Matter* **26**, 125501 (2014).
- [49] S. Lyu and W. R. L. Lambrecht, *Phys. Rev. Materials* **2**, 124602 (2018).